Preparation of Biochar from Rice-Husk for the Adsorption of Methylene Blue in Wastewater

Cynelle Medza-M' Akue[1*],Lianfei Xu[1],Eugloire Charden Goma[2], Pierrick Mezui[3], Vandrice Ovono[4], Russel Allogo[4], Maxime Ondo[4], Boxiong Shen[1]

[1]*Tianjin Key Laboratory of Clean Energy and Pollution Control, Hebei Engineering Research Center of Pollution Control in Power System, School of Energy and Environmental Engineering, Hebei University of Technology, Tianjin, 300131, China*

[2]*School of Mechanical Engineering, Hebei University of Technology, Tianjin, 300131, China*

[3]*EnerjPlus CO., LTD, Dakar 634, Senegal*

[4]*School of Economics and Management, University of Science and Technology of Beijing, Beijing, 100083, China*

**Corresponding Author: cynelle.medza@yahoo.fr*

Abstract: Activated carbon (AC) is a carbon material with a porous structure. It has the characteristics of a large specific surface area, well-developed pore structure, and unique surface functional groups. It is widely used in the field of the pharmaceutical industry, adsorption, energy storage materials, and other fields. Rice husk is a type of widely distributed biomass waste, rich in reserves, renewable, and easy to occur is used to produce activated carbon for the removal of methylene blue (MB). The rice husk is activated with KOH, H_3PO_4, and $ZnCl_2$at different temperatures (600，700 and 800℃). The removal performance of the biochar is investigated such gradually increased to the equilibrium point with increasing adsorption time and increased with increasing activation temperature. The results showed that activated carbon sample prepared with the H_3PO_4 （RHACP700) at 700 ℃has the best removal effect among all the prepared biochar reaching 93.9%. When the pH value was 6, the adsorption effect of activated carbon on methylene blue was the best. In terms of adsorption isotherms, the Langmuir isotherm showed the best results with an R^2 of 0.999and the maximum Q_m was 476.2 mg/g. It was further found that the pseudo-second-order kinetic model was most consistent with the adsorption data of RHACP700, designating the use of the chemical adsorption, which supportsthe results of the FTIR test that shows the presence of −OH, C−H, and C−O functional groups and the XRD that shows the microcrystalline phase in the biochar structure. The material showed a large number of micropores, which is consistent with the adsorption pattern of methylene blue.

Keywords:Activated carbon; biochar; adsorptionisotherm; biomass waste; methylene blue.

Date of Submission: 06-06-2023 Date of acceptance: 08-06-2023

I. INTRODUCTION

Among all sources of energy humanity has, water without any substitute is part of the most important and healthiest for the sustenance of life, for both humans and all species on the planet Earth. Nowadays, one of the biggest challenges human beings are facing is the availability of clean and affordable water(Ormerod & Cooke, 2020).With the rapid development of the textile and dyeing industry, dye wastewater discharge is increasing. According to statistics, China currently discharges more than 900 million tons of textile wastewater each year. Every ton of sewage will cause serious pollution to 20 tons of clean water (Wang Jinyue et al., 2022).

There are a lot of methods for the purification of wastewater such as biological process, chemical oxidation, ozonation, membrane filtration, coagulation, reverse osmosis, photocatalysis, and photo-degradation(Al-Nuaim et al., 2022; Amor et al., 2019; Homocianu & Pascariu, 2022; Nabavi et al., 2023). The biological process has the advantages of low processing cost, slow degradation speed, and large equipment space occupation(Sahoo et al., 2022). The electrochemical method has the advantages of simple equipment, less occupation, and easily achieving automatic control, but the processing cost is high(Alkhadra et al., 2022). Nevertheless, those methods are first of all not effective in the treatment of wastewater containing dye, they are expensive to process and are energy-consuming. Thus, the adsorption has the advantages of simple operation, small occupied area, and good effect, and is the main treatment method of dye wastewater at present.

Adsorption is an earlier method and dyes adsorption is a time-consuming methodeven if a good adsorbent with high capacity is taken for the adsorption although the removal process is fast, the adsorption capacity is greatly high(Islam et al., 2016). Using the adsorption method, the wastewater will be treated better. Its capacity, specific surface area, pore structure, size, surface charge, and surface chemical properties of

activated carbon are closely related to the types and amount of surface functional groups, carbon content, activation mode, activation temperature, and the choice of activator(Kuptajit et al., 2021; Lawtae & Tangsathitkulchai, 2021; S. Li et al., 2022). The adsorbent plays an important role in the removal of dyes in wastewater and activated carbon has proven to be a good material by its excellent characteristics. But, the high-cost preparation of activated carbon limits its implementation.

For that reason, many studies went through the preparation of an adsorbent with low production cost and high adsorption capacity(Chikri et al., 2020; Ho, 2022; Moustafa, 2023; Sulyman et al., 2017). They found that biochar-based adsorbents are good materials that can be used in wastewater purification. The biomass can be prepared from agricultural waste, wood, shells, and many others (Abou-Hadid et al., 2023; Blachnio et al., 2020; Dungani et al., 2022; Gayathiri et al., 2022; Hashemian et al., 2014; Njewa et al., 2022; Pimentel et al., 2023; Yahya et al., 1972). Therefore, for the economic and environmental sake, the preparation of biomass-based activated carbon makes it an excellent adsorbent.

Rice husk is an important by-product of food processing, usually used in feed production or incineration, with low efficiency and low added value(Moraes et al., 2014; Pode, 2016). Therefore, if the rice husk is made into activated carbon with a variety of uses, and then applied to dye wastewater, not only can achieve the purpose of recycling; At the same time, waste treatment, resource recovery, and other goals can be achieved. Bazan-Wozniak Aleksandra et al. obtained high-quality activated carbon through three different heating and activation methods, using H_3PO_4 as the activator. Its specific surface area is more than 520 m^2/g, pore size is uniform, and pore distribution is narrow(Bazan-Wozniak et al., 2022). Sujiono E et al. reacted with NaOH at 600 for 3 hours and then carbonized to obtain rice husk-based activated carbon(Sujiono et al., 2022). The research on activated carbon from rice husk mainly focused on the strong alkaline activation method, which obtained samples with high surface mass fraction, but few products; At the same time, because the dehydration process of hydrogen oxide in the reaction is very violent, and the reaction process is difficult to control, it causes serious corrosion to the reactor. Therefore, it is necessary to find an alternative in the preparation of activated carbon with an easy process, low cost, and which keeps the characteristic of the material even after adsorption.

In this work, rice husk was used as the main raw material, and weak acidic H_3PO_4 and weak basic KOH neutral $ZnCl_2$ were used as activators and were chemically activated at different temperatures. Activated carbon with a well-developed pore structure was obtained. Wang J et al. Chemically prepared the activated carbon from coal using KOH and obtained an adsorbent with a surface area of 165.815 m^2/g (J. Wang et al., 2022). Mbarki F et al. activated the biomass by a chemical activation method using the different activating agents and had an AC with a surface area of 589 m^2/g(Mbarki et al., 2022). Through the adsorption experiments of methylene blue dye, the adsorption characteristics of methylene blue under initial concentration, time, pH, and the adsorption isotherm curves of methylene blue during the adsorption process were studied, which will lay the foundation and theoretical basis for further research.

II. MATERIALS AND METHODS

2.1 Materials

Rice husk is supplied from (Taobo in China), and was used as thematerial precursor. Rice husk was carefully washed with ionized water and then dried in an oven(from Shanghai Yiheng Scientific Instruments Co., Ltd, China),at 105 °C for 12h, which was then pulverized by a multifunctional crusher(supplied by Yongkang Bo Ou Hardware Products Limited Co., Ltd, China). The particles were taken out and screened by a vibrating sieve (supplied by Henan Zhongren Tian Machinery Manufacturing Co., Ltd, China)with 200 meshes to obtain the particles with a diameter of less than 75 μm.

2.2 Methods

2.2.1 Biochar preparation

The material was prepared using chemical activation methods. Firstly, the rice husk was mixed with the chemical reagents (activator), KOH（supplied by Tianjin Kermio Chemical Reagent Co., Ltd.), $ZnCl_2$, and H_3PO_4 (from Aladdin, China), at a mixture ratio of 1:0,1:1; 2:1 (w/w). Afterward, the materials wereput in an ultrasonic vibration machine (Shanghai Lichen Bangxi Instrument Kefa Co., Ltd. China) for 30 minutesunder the condition of 40Hz and 25℃, t then dried at 105 °C for 24 hours. A certain amount (m_1) of the sample was put in a quartz boat, which was next put in a tube furnace (Hefei Crystal Materials Technology Co., Ltd. China). Under N_2atmosphere (600 mL/min), the temperature was increased to a target value at a rate of 10 °C/min, kept constant for 1 hour, and then decreased to room temperature. The activation process was carried out at the target temperatures of 600, 700, and 800 °C.

After the activation, the prepared biochar was cleaned with 1 mol/L NaOH solution(for H_3PO_4 activated samples) and HCl (supplied by Tianjin Kermio Chemical Reagent Co., Ltd), and thenwashed repeatedly with

ionized water until its filter solution reached neutral. The washed biochar was dried in an electric blast drying oven at 105 °C until completely dried and then weighed (m_2). The rice husk-based biochar activated with no activator, KOH, $ZnCl_2$, and H_3PO_4 were labeled as RHAC, RHACK, RHACZ ,and RHACP, respectively. The yield of biochar, X, is calculated by Equation (1).

$$X = (m_2/m_1) \times 100\% \quad (1)$$

2.2.2 Adsorption experiment

MB was used as an adsorbate in this study. With a characteristic absorption wavelength of 664 nm, the absorbance of MB aqueous solutions at various concentrations was measured using a UV spectrophotometer. The concentration-absorbance coordinate axis was used to plot the data, and a linear regression equation （2） with a fitting coefficient of 0.999 worked well to fit the data.

$$y = 14.29x - 0.3163 \quad (2)$$

A 10 mg/L MB solution was prepared and used to demonstrate the efficiency of biochar. processing. A certain amount of rice bran biochar was added to 50 mL of MB solution, and the pH value of the solution was adjusted to neutral using 0.1 mol/L NaOH and HCl solution. The sample was separated and samples were taken after the same reaction time. The sampling time was set at 0, 10, 20, 30, 40, 50, 60, and 70 min, and the sample concentration was measured with a UV spectrophotometer. At arbitrary reaction times (min), the Adsorption rate, R, and the adsorption capacity, (mg/g), were calculated according to formulas (3) and (4).

$$R = (C_0 - C_t)/C_0 \times 100\% \quad (3)$$

$$q_t = (C_0 - C_t)V/m (4)$$

Where C_0 and C_t are the concentrations of MB (mg/L) before and after adsorption, respectively, V is the solution volume, and m is the amount of adsorbent (g).

2.2.3 Characterization of biochar

The surface modification of biochar with different loading ratios was determined by SEM (ESCANCLARA). The surface functional groups of the raw material and modified biochar were characterized by FTIR (DTGSKBR). Measurements for both samples were taken in the numerical range of 500─4000 cm^{-1} with a temperature dependence at a resolution of 4 cm^{-1}. Nitrogen isotherms were performed at 77 K using an ASAP2460 surface area and microporous analyzer. The Brunauer-Emmett-Teller (BET) equations and the nonlocal density functional theory method were used to obtain the specific area and volume of species distributions before and after the transformations.

2.2.4 Adsorption isotherm type

The parameters obtained from isotherm modeling provide important information about the adsorption mechanism, surface properties, and adsorbent-adsorbate affinities. The two most commonly used models are those of Langmuir and Freundlich.

(1) Langmuir model

This model is very useful for the mono-molecular adsorption of a solute by forming a monolayer on the surface of an adsorbent, and is used when the following conditions are met: the adsorbed species is fixed on a single well-defined site, each site is only capable of fixing one adsorbed species, the adsorption energy of all the sites is identical and independent of other species already adsorbed on neighboring sites (Hu et al., 2007)(Kalam et al., 2021).It is described by the following expression:

$$\frac{C_e}{q_e} = \frac{1}{k_L q_m} + \frac{C_e}{q_m} (5)$$

Whereq_e is the adsorption capacityq_m is the maximum adsorption capacity, $C_e$is equilibrium concentration,and k_L is Langmuir's constant (L/mg).The coefficients of the model ($k_L$and q_m) can be obtained

from the linear plot of C_e/q_e as a function of C_e.

(2) Freundlich model

Freundlich's empirical model is based on adsorption onto heterogeneous surfaces(Hambisa et al., 2023; Hasani et al., 2022).The Freundlich isotherm is given in its linear form by:

$$lnq_e = lnk_F + \frac{1}{n} lnC_e (6)$$

Where k_F is the Freundlich coefficient representing the adsorption capacity (mg/g.(L/mg)1/n) and n is the Freundlich coefficient representing the adsorption intensity. The Freundlich coefficients (k_F and n) can be obtained from the linear plot of $\ln(q_e)$ as a function of $\ln(c_e)$.

2.2.5 Adsorption Theoretical model

(1) Pseudo-first order kinetic model

This model can be used to describe the phenomena that occur during the first few minutes of the adsorption process(Fathi Hasanbarogh et al., 2022; Keleşoğlu et al., 2012; Lestari et al., 2022; Ugraskan et al., 2022), as given in equations (7) and (8).

$$\frac{dq_t}{dt} = k_1(q_e - q_t) (7)$$

Where q_e is the equilibrium adsorption capacity (mg/g), and k_1 is the pseudo-first-order kinetic adsorption rate constant, g/(mg·min).

$$q_e = (C_0 - C_e)V/m (8)$$

Where C_e is the equilibrium concentration of MB after adsorption (mg/L).

(2) Pseudo-second order kinetic model

Unlike the first-order model, the pseudo-second-order model is applicable to a wider time interval (generally the entire adsorption process). It includes the solution concentration, pH, temperature, adsorbent, and ionic strength(Abbas & Trari, 2020; Kyzas et al., 2016; X. Li et al., 2020; Touzani et al., 2022; Y. X. Wang et al., 2015). And it's given in equation (9).

$$\frac{dq_t}{dt} = k_2(q_e - q_t)^2 (9)$$

Where $k_2$is the second-order reaction rate constant for the adsorption of MB onto AC (g/mg/min). q_e is the quantity adsorbed at equilibrium (mg/g). q_t is the quantity adsorbed at time t (mg/g). t is the contact time (min).

(3) Elovich kinetic model

The model, as given in equation (10), is suitable for describing the process of adsorption reaching equilibrium rapidly in the early stage and slowing down in the late stage(Đurović-Pejčev et al., 2023; Han et al., 2020; Zhang et al., 2023).

$$\frac{dq_t}{dt} = a \times \exp^{(-bt)} (10)$$

Where a is the initial adsorption rate constant, g/(mg·min^2), and b is the desorption constant, g/(mg·min).

(4) Intra-particle diffusion kinetic model

The MB molecules are probably transported into the adsorbent particles by a process of intra-particular diffusion due to the porosity of the activated carbons.Generally, three steps are involved during the adsorption process by the porous adsorbent: 1） transfer of the adsorbed molecule from within the solution to the external surface of the adsorbent (external diffusion).2） Penetration of the adsorbed molecule inside the pores of the adsorbent (intra-particle diffusion, within the pores). 3) adsorption of the molecule on the internal pore surface(Gürkan et al., 2021, 2022; Zhang et al., 2023). The model, as given in equation (11):

$$q_t = C + {K_{pt}}^{0.5} (11)$$

Where K_{pt} is the internal diffusion rate constant, mg/(g·min$^{0.5}$).

III. RESULT AND DISCUSSION

3.1 Biochar yield

The biochar yield calculated by weighing and calculation is shown in **Figure 1** below. After analysis, it can be seen that, compared with the control group, the experimental group at the corresponding temperature of activated carbon yield is only higher at the H_3PO_4 activation group which had the largest difference in the yield of 10.9% and 26.58% respectively, under different activation temperatures. On the whole, the H_3PO_4 activated group in the experimental group has the highest overall yield, especially at 600°C temperature, the yield of biomass charcoal obtained by activation is significantly higher than the same temperature activated by the other two activators.

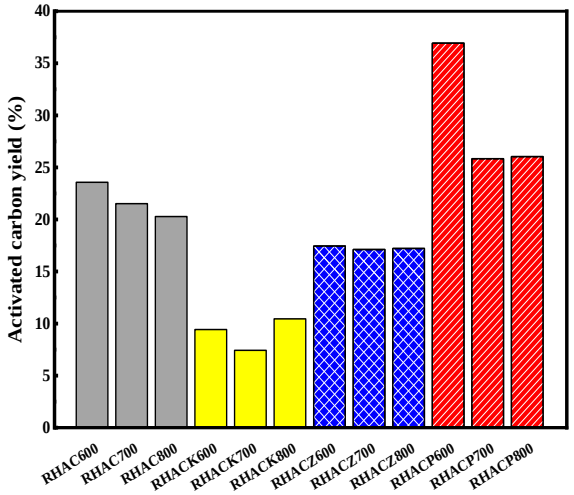

Figure 1: Completed circuit of the hybrid power control system. Yields of biochar from pyrolysis and activation of the rice husk. (Experimental conditions: MB concentration:50 mL, 10 mg/L, adsorbent dosage: 50mg, contact time 70 min).

3.2 Removal of methylene blue by biochar

Adsorption performances of the three groups of biochar towards MB were explored, i.e., RHAC600, RHAC700, and RHAC800; for the experimental group which includes, KOH activated group: RHACK600, RHACK700 and RHACK800; $ZnCl_2$ activated group: RHACZ600, RHACZ700, RHACZ800; H_3PO_4 activated group: RHACP600, RHACP700 and RHACP800. Effects of activation temperature, pH, activator and OPACZ600 loading were assessed.

3.2.1Effect of activation temperature

As can be seen in **Figure 2**(a), the removal rate of methylene blue by the biochar in the control group was less than 50 %, and increase with increasing activation temperature. This may be attributed to the pores generated in the resulting carbon. For the removal rate of the KOH activation group**Figure 2**(b), also showed an increase with the increasing temperature. The removal rate for the $ZnCl_2$ activation group**Figure 2**(c) showed a similar trend to that for the H_3PO_4 activation group, i.e., increased with the increasing activation temperature, and increased with adsorption time then tended to be flat. About the H_3PO_4 activation group**Figure 2**(d), the removal rate of methylene blue increased with adsorption time and reached a maximum of 40 minutes. The final removal rate was between 86 and 93 % and also increased with the increasing activation temperature. However, it took only 30 minutes for the removal rate of the control group, the KOH activation group and the $ZnCl_2$ activation group to reach the maximum, which is less than 40 minutes for the H_3PO_4 activated group, indicating that the adsorptions of methylene blue by activated biochar were easier to reach equilibrium.

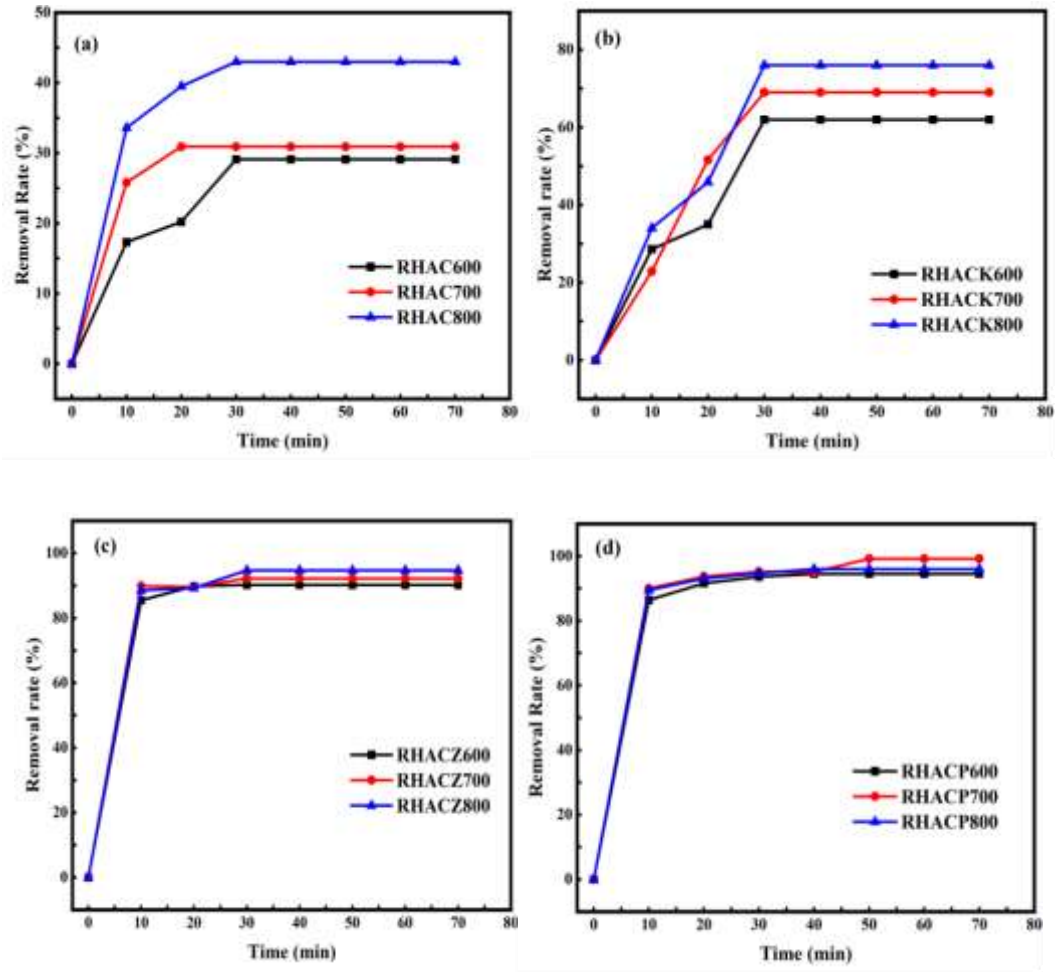

Figure 2. Activation temperatures effect on adsorption of methylene blue by AC in (a) the control group, (b) the KOH activation group; (c) the $ZnCl_2$ activation group, and (d) the H_3PO_4 activation group.(Experimental conditions: MB concentration:50 mL, 10 mg/L, adsorbent dosage: 50mg, contact time 70 min).

3.2.2 Effect of pH

The effect of methylene blue solution pH on methylene blue removal is shown in **Figure 3**. It can be seen that when the methylene blue solution is strongly acidic (pH=2), the removal rate of methylene blue is 96.67%, but when the solution is close to neutral (pH=6), the removal rate of methylene blue reaches the maximum of 99.89%, and when the solution becomes strong alkaline, the removal rate of methylene blue hardly changes. This is mainly because, in the methylene blue solution in the acidic environment, the positive charge of the group will hinder the dye absorption, but in the neutral state, it will produce a double charge, so its polarity changes; The results show that the removal rate of methylene blue is improved.

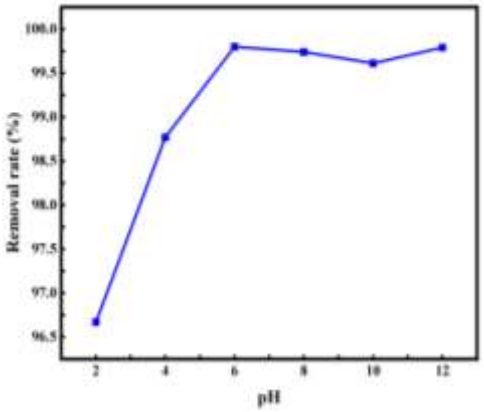

Figure 3. Effect of pH value on methylene blue removal rate(Experimental conditions: MB concentration:50 mL, 10 mg/L, adsorbent dosage: 50mg, contact time 70 min).

3.2.3 Effect of Activators

The optimal samples in each group, i.e., biochar prepared at 700 ℃, are compared in **Figure 4**. Compared with the RHAC700, the RHACK700, RHACZ700, and RHACP700 displayed a high removal rate of methylene blue. The RHACP700 had a faster adsorption rate at the initial stage of adsorption than the other groups and had the higher adsorption rate, this result can be attached to the material excellent surface properties.

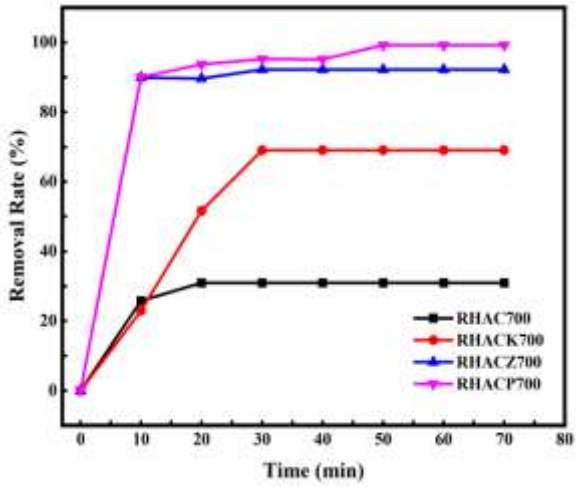

Figure 4. Effect of theactivator on the removal rate of MB.(Experimental conditions: MB concentration:50 mL, 10 mg/L, adsorbent dosage: 50mg, contact time 70 min).

3.2.4 Effect of OPACZ600 dosage

The RHACP700 has the highest removal rate of methylene blue. The effects of the RHACP700 dosage on the adsorption of methylene blue by biochar was explored. **Figure 5** shows that the dosage amount of AC had a huge impact on the removal rate and the adsorption equilibrium time, those results can be due to the increase in the surface area and the availability of active sites. As the RHACP700 dosage increased from 10mg-80mg, the removal rate curve showed a fast and big increase while a small effect has been observed when more biochar is added. The adsorption equilibrium time was 20 minutes at the RHACP700 dosage of 10 and 20 mg and increased to 40 minutes as the RHACP700 dosage further increased. For the economical sake and removal rate of methylene blue, 80 mg activated carbon per 50 mL methylene blue solution (10 mg/L) was selected.

Wherefore, it is found in the literature that a lot of research on the removal of dye by biochar-based rice husk is done using the adsorption method but the proper activation process is yet to be found. El-Shafey et al. produced the activated carbon from rice husk treated with sulfuric acid for the removal of Cd (II) and Se (IV), the adsorption was found to be low and reaching equilibrium after 2h and 200h respectively (El-Shafey, 2007). Ahiduzzaman et al. prepared the activated carbon from rice husk using zinc chloride, the adsorption was good and the material had a well-developed micropore structure. However, these methods had certain problems of aggressive corrosion, chemical recovery, and other environmental disadvantages. Thus, using rice-husk based activated carbon treated with phosphoric acid has better advantages like a high surface area, high and fast adsorption rate, it is economically favorable, gives a better yield.

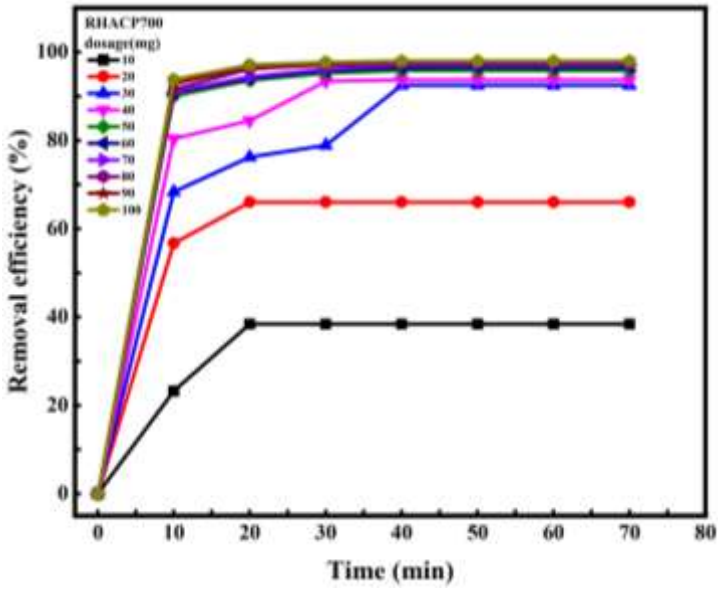

Figure 5. Effects of the RHACP700dosage on the removal of methylene blue. (Experimental conditions: MB concentration:50 mL, 10 mg/L, adsorbent dosage: 50mg, contact time 70 min).

3.3 Adsorption isotherm model

(1) Langmuir model isotherm is represented in the **Figure 6.**

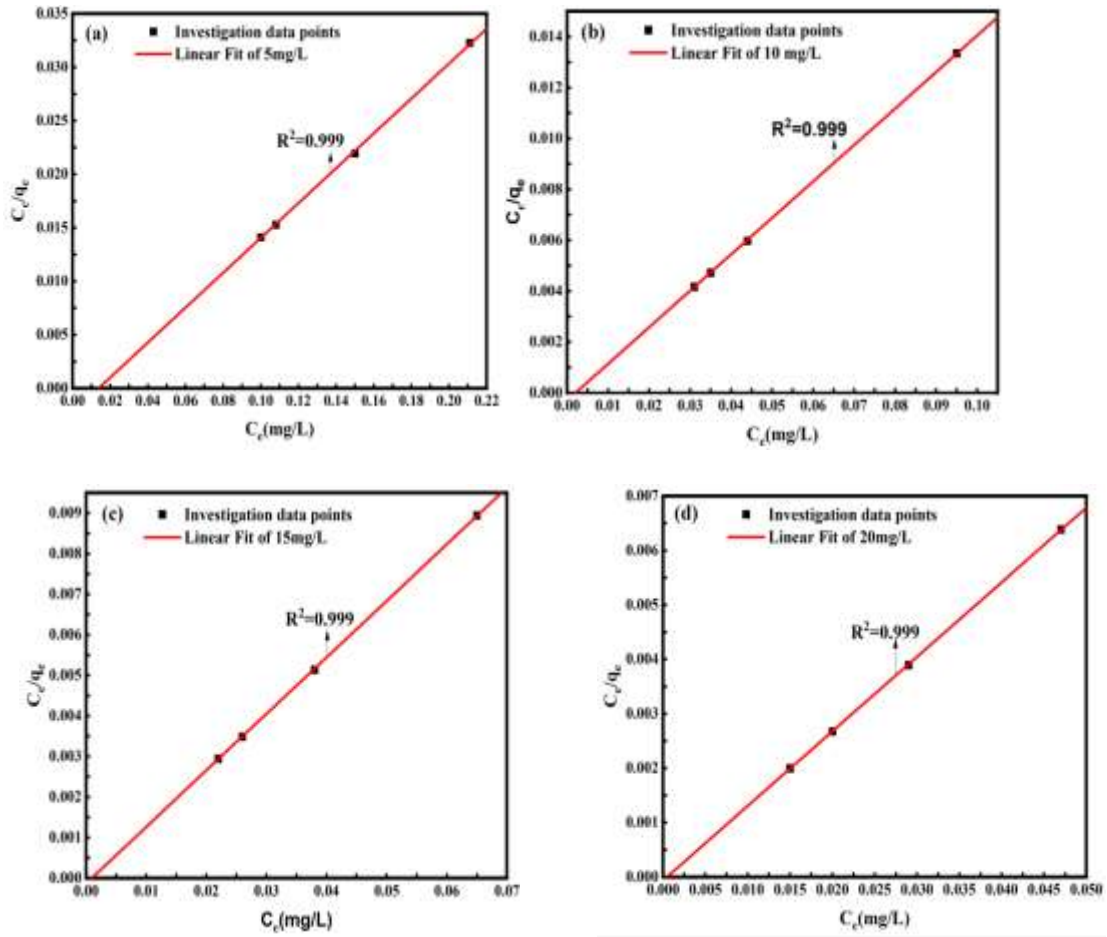

Figure 6.Freundlich isotherm model(a) RHACP700 5mg/L, (b) RHACP700 10mg/L, (c) RHACP700 15mg/L and (d) RHACP700 20mg/L. (Experimental conditions: MB concentration:50 mL, 10 mg/L, adsorbent dosage: 50mg, contact time 70 min).

Table 1. Fitting results of Langmuir and Freundlichisotherm

C_0	Langmuir Isotherm			Freundlich Isotherm		
	K_L	q_{max}	R^2	K_F	1/n	R^2
5	0.59	476.2	0.999	313.4	0.093	0.989
10	0.54	456.6	0.999	298.7	0.087	0.987
15	0.42	421.5	0.999	280.4	0.062	0.926
20	0.38	448.4	0.999	237.1	0.08	0.852

The adsorption of methylene blue by rice husk-based activated carbon is a dynamic process. The Langmuir and Freundlich equations describing the solid-liquid adsorption isotherms are usually used to study the adsorption mechanism. Langmuir isotherm is assumed to be a single molecular layer, i.e., the energy of each adsorption site is the same. From Figure 5 and Figure 6 it shows thatthe material followed the Langmuir model and the experimental data were fitted, and the results shown in **Table 1**indicate the correlation coefficient R^2 (0.9999) for the four samples that are larger than Freundlich (0.989,0.987,0.926,0.852), which shows that the adsorption isotherms of rice husk activated carbon on methylene blue are in good agreement with the Langmuir isotherms and that the formation of a monolayer on the sorbent surface gives better results than other models. Futhermore, the adsorption happens on homogeneous surfaces. From the literature, many researches on the adsorption isotherm obtained the best results fitted with Langmuir model. Seyyed Alireza Moussavi et al. Prepared activated carbon from grape wood and reached qmax= 5.88 mg/g(Mousavi et al., 2022). Jiwon Chung et al. with an activated carbon from sucrose and melamine observed a maximum MB adsorption of 476.190 mg/g (Chung et al., 2022).

3.4 Adsorption kinetics

In order to demonstrate the type or order of MB retention kinetics by RHACP700, four models were tested. It can be seen from **Figure 7** that adsorption curves of the RHACP700 towards MB are abrupt, which indicates that the adsorption rates are fast due to the accumulation of the adsorption sites in the material. The adsorption capacity significantly increases when the concentration of MB increases from 5 mg/L - 10 mg/L, but then no longer change when the concentration increases, these results can be explained by the which may be due to lacking of adsorption sites in RHACP700. Furthermore, the concentration of MB decreases while the adsorption time rise, and the curves tend to be flat, reaching after 40 minutes an equilibrium of MB adsorption and desorption. The adsorption rate is fast and is marked as 90% to 100% of the total adsorption amount in the first 40 minutes.

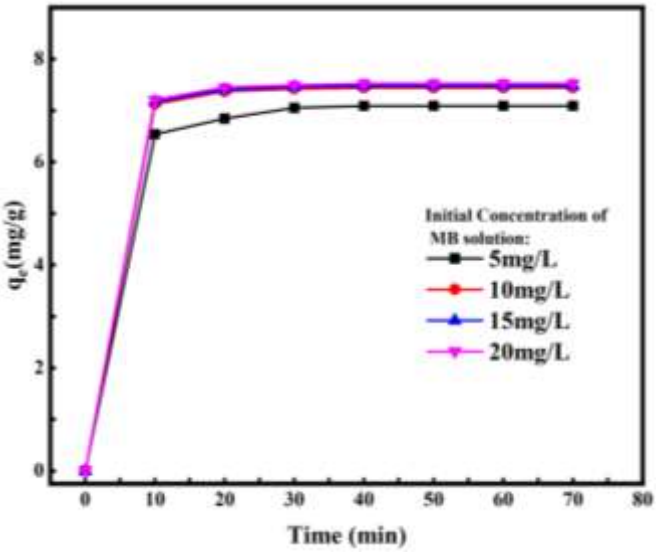

Figure 7. Effects of initial concentration of methylene blue on its adsorption by RHAP700.(Experimental conditions: MB concentration:50 mL, 10 mg/L, adsorbent dosage: 50mg, contact time 70 min).

To procure more information on the adsorption process, the Pseudo-first order, Pseudo-second order, Elovich model and Intra-particle diffusion kinetic model are applied to fit the data in **Figure 7**. The lines obtained by fitting adsorption data with the four models are expressed in **Figure 8**, and their parameters are obtained as well as presented in **Table 2**. The models have fitting coefficients of 0.850-0.923, 0.999-1, 0.941-0.988 and 0.938-0.986 for the Pseudo-first, the Pseudo-second order, the Elovich model and Intra-particle diffusion kinetic model, respectively. Among the four kinetic models, the Pseudo-second order kenetic model has the greatest fitting degree which specifies that throughout the adsorption process of MB by RHACP700, the chemical adsorption take place.

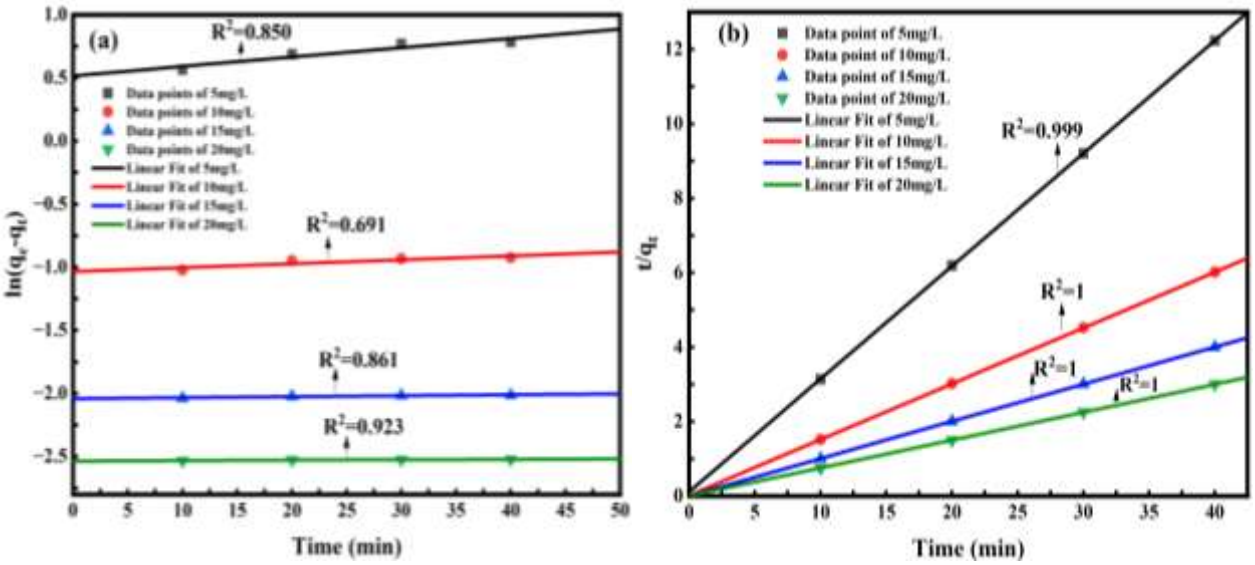

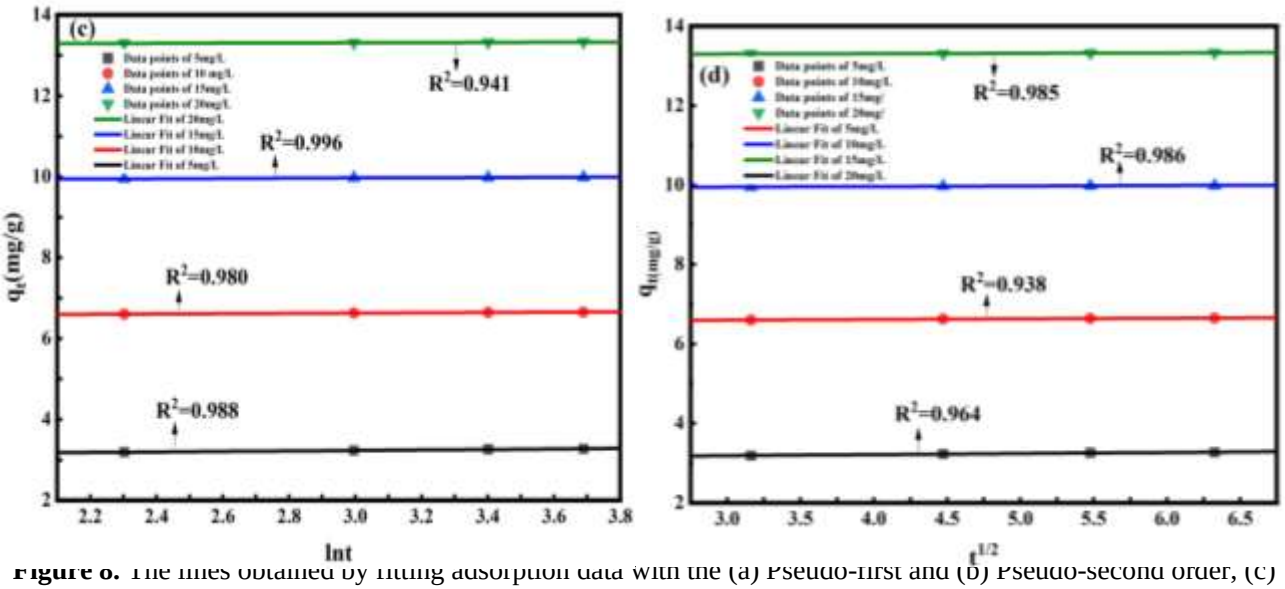

Figure 8. The lines obtained by fitting adsorption data with the (a) Pseudo-first and (b) Pseudo-second order, (c) Elovich and (d)Intra-particle diffusion kinetic models. (Experimental conditions: MB concentration:50 mL, 10 mg/L, adsorbent dosage: 50mg, contact time 70 min).

Table 2. Parameters obtained from the fitted results of adsorption data by the four kinetic models

C_0	q_e(exp)	Pseudo-first order			Pseudo-second order			Elovich			Intra-particle diffusion		
		R^2	q_e	K_1 (10^{-4})	R^2	q_e	K_2	R^2	β	α	R^2	c	$K_{pt}^{\frac{1}{2}}$
5	7.09	0.850	1.67	1.84	0.999	3.3	0.0381	0.988	0.181	16.78	0.964	3.11	0.02609
10	7.44	0.691	2.81	7.75^5	1	6.66	1.412	0.980	0.232	28	0.938	6.55	0.01554
15	7.48	0.861	7.69	1.84	1	1.0003	165.73	0.996	0.28	35.23	0.986	9.91	0.01249
20	7.52	0.923	12.62	8.3	1	13.34	1.992	0.941	0.278	47.50	0.985	13.26	0.00944

3. Characterization and analysis of biochar

3.1 Pore structure analysis

The pore structure of RHAC700 and RHACP700 were obtained based on the N_2 adsorption-desorption isotherms. RHAC700 showed a Type I isotherm which is the trait of a microporous material, as shown in **Figure 9**(a). The N_2 adsorption capacity was less than 50 cm3 g^{-1}, this indicated that the devolatilization only played a little part in the pore structure, which was consistent with the surface morphology shown in **Figure 10**. The RHACP700 revealed a combination of type I and type IV isotherms with a small H4-type hysteresis loop, indicating that there are large amounts of microcores and some mesopores(Mu et al., 2020). The specific surface area and total pore volume of RHACP700 reached 568.9132 m^2/g and 0.368723 cm3 g^{-1} respectively as displayed in **Table 3**.

The pore distribution of the samples was calculated, as shown in **Figure 9** (b). RHAC700 and RHACP700 had high-rise volumes in the micropore from 0.5−2 nm. The pores in RHAC700 are mostly micropores of 1.1−1.4 nm. Ensuing the activation, some micropores were carve into large pores, followed by the creation of large numbers of smaller pores. Between 0.5−0.9 nm, RHACP700 had a large micropore volume, pores below 1 nm which mainly contribute to the specific capacitance. The RHACP700 showed pore structure, which are suitable for adsorbing methylene blue molecules with larger molecular diameters. There are a large number of micropores, and it takes a long time to reach adsorption equilibrium, which is consistent with the adsorption law of methylene blue(Pelekani & Snoeyink, 2000).

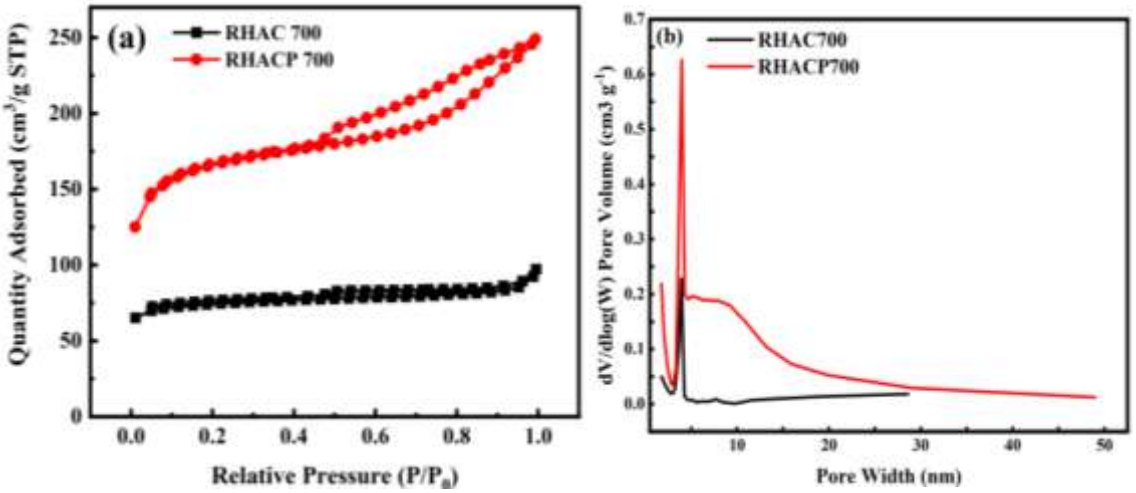

Figure 9. (a) N_2 adsorption-desorption isotherms and (b) pore distributions of theRHAC700 and RHACP700.

Table 3. Specific surface areas and pore volumes of the biochars.

Sample	S_{BET} (m^2/g)	$S_{Mesopore}$ (m^2/g)	$S_{Micropore}$ (m^2/g)	V_{Total} (cm^3/g)	$V_{Mesopore}$ (cm^3/g)	$V_{Micropore}$ (cm^3/g)
RHAC700	256.0468	45.4894	210.5575	0.131864	0.037086	0.094778
RHACP700	568.9132	169.8965	399.0167	0.368723	0.187392	0.181331

3.2 Surface morphology analysis

Figure 10a-f shows SEM images of the RHAC700 and RHACP700.The RHAC700 were quite smooth and did not have many pores. After activation of RHAC700 with H_3PO_4 we remark that numerous pores appeared on the materials and the surface porosity of the materials crucially increased, as shown in the **Figure 10** (d)-(f). The center of pore on RHACP700 surface was darker, which specify that the pore structure was cavernous in the carbon matrix compared to the surface(Kim et al., 2019)which is aligned with the results obtained by BET analysis in **Figure 9**. It proves that the adsorption capacity of the materials to methylene blue molecules will be enhanced after activation.

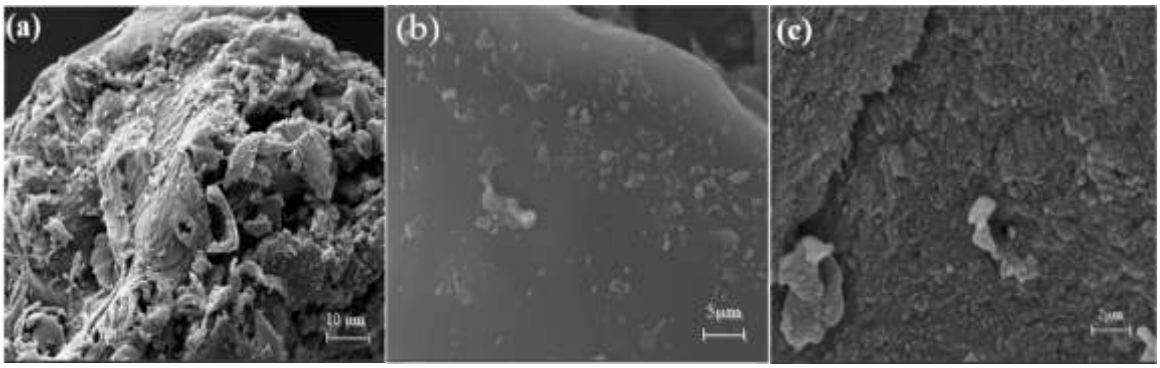

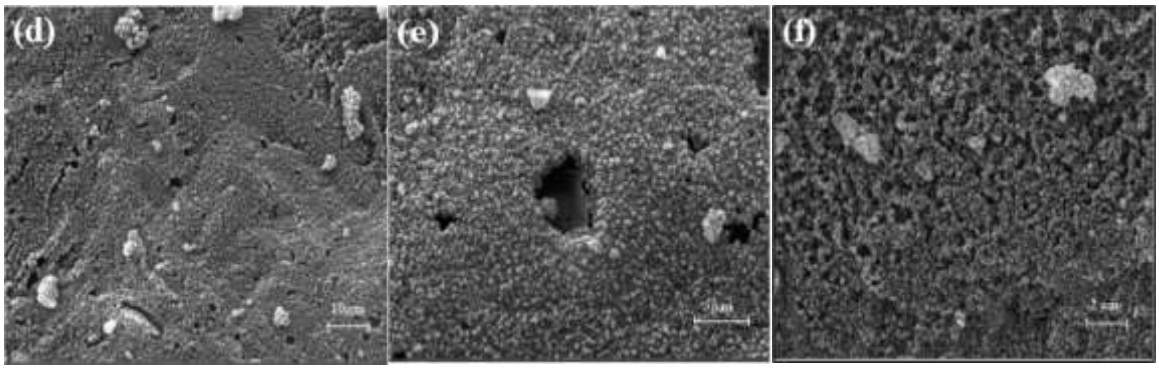

Figure 10. SEM images of (a), (b) and (c) the RHAC700; and (d), (e) and (f) the RHACP700

3.3 Surface functional group analysis

To understand more about the structure of the samples, FTIR spectra of the two materials were revealed in **Figure 11**. From **Figure 11**, the samples showed significant absorption peaks at 3406.57 which associated with the elongation movement of the O−H indicates the presence of the hydroxyl group (−OH) and chemisorbed water. The peaks at1184.28 ,1097.05 and 1039.83 correspond to the C−O elongation movement of the carbonyl group which may indicate the presence of carboxylic acids(Ahmad et al., 2021). The peaks at 798.50, 710.67, 677.13, 501.71 and 465.66 cm^{-1} correspond to the C−H deformation vibrations in benzene derivatives.

It can be seen from the Figure that RHACP700 has higher absorption peaks from peak, indicating that the activated RHACP700 has more C−O and −OH functional groups. Compared with RHAC700, RHAC700 has more absorption peaks indicating that it has more aromatic hydrocarbons which may be due to the etching of a large amount of amorphous carbon in the char.

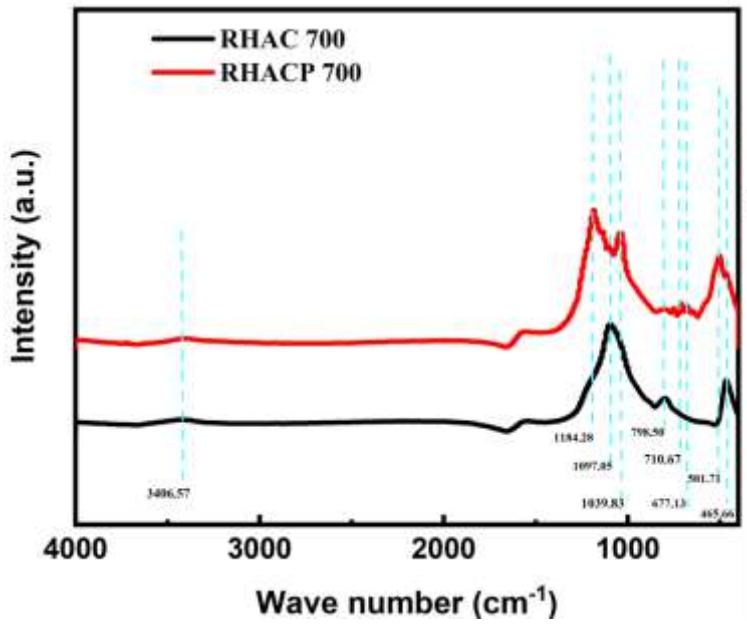

Figure 11. FTIR spectra of RHAC700 and RHACP700

3.4 X-Ray Powder Diffraction (XRD)

Figure 12 displays the results acquired from the XRD analysis. From the AC XRD results, **Figure 12** revealed peaks at 2θ= 23° and 44° corresponding to those of a carbonaceous material like activated carbon.These peaks around 23° and 44° can be attributed to the reflection of the graphite (002) and (100) respectively. The peak 2θ = 23° is a trait of the cellulose which is attributed to the crystalline phase in the structure of the AC(Shaaban et al., 2013). The peaks between 20˚–30˚ correspond to the stacking structure of the aromatic layers (graphite 002), while the (100) peak indicates the honeycomb structures formed by carbons. This result is in agreement with the SEM images of these activated carbons (**Figure 10**). The RHACP700

showed a keener (002) peak than the RHAC700, indicating a neat agglomeration of aromatic layer during its activation process. RHACP700 had a faintly higher (100) peak than the other, indicated a small increase in the size of aromatic layer. RHACP700 has additional peaks appeared at 2θ = 27˚ which constitute the crystalline SiO_2(Liu et al., 2012; Takagi et al., 2004).

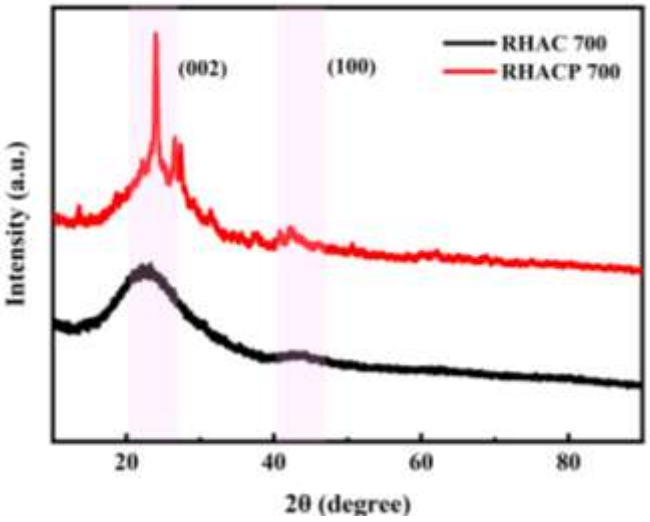

Figure 12. XRD patterns of RHAC700 and RHACP700

IV. CONCLUSION

This work presents the preparation of biochar from rice husk activated by KOH, $ZnCl_2$ and H_3PO_4at 600, 700 and 800 ℃. The adsorption performance and different parameters of the prepared activated carbon on MB was assessed.

(1) TheRHACP700 showsa higher biochar yield than others. The removal rates of MB by the biochar increase with the increase of theactivation temperature. The time required for the H_3PO_4activation group to reach adsorption equilibrium is less than of the $ZnCl_2$activation group, while the RHACP later shows a higher final removal rate. And the removal rate of MB increases as the pH further increases.

(2) As the dosage of the RHACP700 to MB solution increases, both the removal rate and the adsorption equilibrium time show a significant increase followed by a decrease in growth rate. An optimal condition of 80 mg biochar per 50 mL MB solution (10 mg/L) is obtained with a removal rate of 98.6 %.

(3) The adsorption isotherm of activated carbon from rice husk on methylene blue was consistent with the Langmuir isotherm model, and the Q_m of activated carbon from rice husk was 476.2 mg/g which infer that the adsorption process of MB using rice husk take place on homogeneous surfaces, while there is no interaction between the adsorbed molecules meaning that the adsorption process happens physically. And the Pseudo-second order adsorption kinetic model fits best (R^2=1) with adsorption data of the RHACP700 towards MB among the four models, indicating presence of the chemical adsorption, which is consistent with the FTIR results that the RHACP700 contains more C−O and −OH functional groups.

(4) The porous surface with large amounts of micropores and some mesopores, and the high specific surface (1199.20 m^2/g) and the XRD shows in general an amorphous structure and a quite high crystallinity of the samples in the range from 23 to 44^o which also contribute to the adsorption of MB by the RHACP700.

REFERENCES

[1] Ormerod, S. J., & Cooke, S. J. (2020). Conservation Challenges to Freshwater Ecosystems. *Encyclopedia of the World's Biomes*, *4*, 270–278. https://doi.org/10.1016/B978-0-12-409548-9.11937-2.

[2] Wang Jinyue, Ding Bingxue, & Zhang Li. (2022). Preparation of activated carbon from rice husk sludge and its adsorption properties. *Chemical Engineering*, *36*(3), 5. https://doi.org/10.3390/POLYM9080370.

[3] Homocianu, M., & Pascariu, P. (2022). High-performance photocatalytic membranes for water purification in relation to environmental and operational parameters. *Journal of Environmental Management*, *311*, 114817. https://doi.org/10.1016/j.jenvman.2022.114817.

[4] Al-Nuaim, M. A., Alwasiti, A. A., & Shnain, Z. Y. (2022). The photocatalytic process in the treatment of polluted water. *Chemical Papers 2022 77:2*, *77*(2), 677–701. https://doi.org/10.1007/S11696-022-02468-7.

[5] Amor, C., Marchão, L., Lucas, M. S., & Peres, J. A. (2019). Application of Advanced Oxidation Processes for the Treatment of Recalcitrant Agro-Industrial Wastewater: A Review. *Water 2019, Vol. 11, Page 205*, *11*(2), 205. https://doi.org/10.3390/W11020205.

[6] Nabavi, E., Pourrostami Niavol, K., Dezvareh, G. A., & Khodadadi Darban, A. (2023). A combined treatment system of O3/UV oxidation and activated carbon adsorption: emerging contaminants in hospital wastewater. *Journal of Water and Health*, *21*(4), 463–490. https://doi.org/10.2166/WH.2023.213.

[7] Sahoo, A. K., Dahiya, A., & Patel, B. K. (2022). Biological methods for textile dyes removal from wastewaters. *Development in Wastewater Treatment Research and Processes*, 127–151. https://doi.org/10.1016/B978-0-323-85657-7.00009-2.

[8] Alkhadra, M. A., Su, X., Suss, M. E., Tian, H., Guyes, E. N., Shocron, A. N., Conforti, K. M., De Souza, J. P., Kim, N., Tedesco, M., Khoiruddin, K., Wenten, I. G., Santiago, J. G., Hatton, T. A., & Bazant, M. Z. (2022). Electrochemical Methods for Water Purification, Ion Separations, and Energy Conversion. *Chemical Reviews*, *122*(16), 13547–13635. https://doi.org/10.1021/ACS.CHEMREV.1C00396/ASSET/IMAGES/MEDIUM/CR1C00396_0032.GIF.

[9] Islam, S. M. D. U., Majumder, R. K., Uddin, M. J., Khalil, M. I., & Ferdous Alam, M. (2016). Hydrochemical Characteristics and Quality Assessment of Groundwater in Patuakhali District, Southern Coastal Region of Bangladesh. *Exposure and Health*, *1*(9), 43–60. https://doi.org/10.1007/S12403-016-0221-Y.

[10] Kuptajit, P., Sano, N., Nakagawa, K., & Suzuki, T. (2021). A study on pore formation of high surface area activated carbon prepared by microwave-induced plasma with KOH (MiWP-KOH) activation: Effect of temperature-elevation rate. *Chemical Engineering and Processing - Process Intensification*, *167*, 108511. https://doi.org/10.1016/J.CEP.2021.108511.

[11] Li, S., Tan, X., Li, H., Gao, Y., Wang, Q., Li, G., & Guo, M. (2022). Investigation on pore structure regulation of activated carbon derived from sargassum and its application in supercapacitor. *Scientific Reports 2022 12:1*, *12*(1), 1–17. https://doi.org/10.1038/s41598-022-14214-w.

[12] Lawtae, P., & Tangsathitkulchai, C. (2021). The Use of High Surface Area Mesoporous-Activated Carbon from Longan Seed Biomass for Increasing Capacity and Kinetics of Methylene Blue Adsorption from Aqueous Solution. *Molecules*, *26*(21). https://doi.org/10.3390/MOLECULES26216521.

[13] Moustafa, M. T. (2023). Preparation and characterization of low-cost adsorbents for the efficient removal of malachite green using response surface modeling and reusability studies. *Scientific Reports 2023 13:1*, *13*(1), 1–33. https://doi.org/10.1038/s41598-023-31391-4.

[14] Ho, S. (2022). Low-Cost Adsorbents for the Removal of Phenol/Phenolics, Pesticides, and Dyes from Wastewater Systems: A Review. *Water 2022, Vol. 14, Page 3203*, *14*(20), 3203. https://doi.org/10.3390/W14203203.

[15] Chikri, R., Elhadiri, N., Benchanaa, M., & El maguana, Y. (2020). Efficiency of sawdust as low-cost adsorbent for dyes removal. *Journal of Chemistry*, *2020*. https://doi.org/10.1155/2020/8813420.

[16] Sulyman, M., Namiesnik, J., & Gierak, A. (2017). Low-cost Adsorbents Derived from Agricultural By-products/Wastes for Enhancing Contaminant Uptakes from Wastewater: A Review. *Polish Journal of Environmental Studies*, *26*(2), 479–510. https://doi.org/10.15244/PJOES/66769.

[17] Abou-Hadid, A. F., El-Behairy, U. A., Elmalih, M. M., Amdeha, E., Naggar, A. M. A. E., Taha, M. H., & Hussein, A. E. M. (2023). Conversion of corn shell as biomass solid waste into carbon species for efficient decontamination of wastewater via heavy metals adsorption. *Biomass Conversion and Biorefinery*, *1*, 1–15. https://doi.org/10.1007/S13399-023-04057-4/FIGURES/12.

[18] Blachnio, M., Derylo-Marczewska, A., Charmas, B., Zienkiewicz-Strzalka, M., Bogatyrov, V., & Galaburda, M. (2020). Activated Carbon from Agricultural Wastes for Adsorption of Organic Pollutants. *Molecules*, *25*(21). https://doi.org/10.3390/MOLECULES25215105.

[19] Gayathiri, M., Pulingam, T., Lee, K. T., & Sudesh, K. (2022). Activated carbon from biomass waste precursors: Factors affecting production and adsorption mechanism. *Chemosphere*, *294*, 133764. https://doi.org/10.1016/J.CHEMOSPHERE.2022.133764.

[20] Hashemian, S., Salari, K., & Yazdi, Z. A. (2014). Preparation of activated carbon from agricultural wastes (almond shell and orange peel) for adsorption of 2-pic from aqueous solution. *Journal of Industrial and Engineering Chemistry*, *20*(4), 1892–1900. https://doi.org/10.1016/J.JIEC.2013.09.009.

[21] Pimentel, C. H., Freire, M. S., Gómez-Díaz, D., & González-Álvarez, J. (2023). Preparation of activated carbon from pine (Pinus radiata) sawdust by chemical activation with zinc chloride for wood dye adsorption. *Biomass Conversion and Biorefinery 2023*, *1*, 1–19. https://doi.org/10.1007/S13399-023-04138-4.

[22] Yahya, M. A., Mansor, M. H., Auji, W. A., Zolkarnaini, W., Rusli, S., Aminuddin, A., Mohamad, K., Aina, F., Sabhan, M., Abdallah, A., Atik, A., Ozair, L. N., & Rusli, N. S. (1972). *A brief review on activated carbon derived from agriculture by-product AIP Conference*. 20129. https://doi.org/10.1063/1.5041244.

[23] Njewa, J. B., Vunain, E., & Biswick, T. (2022). Synthesis and Characterization of Activated Carbons Prepared from Agro-Wastes by Chemical Activation. *Journal of Chemistry*, *2022*. https://doi.org/10.1155/2022/9975444.

[24] Dungani, R., Munawar, S. S., Karliati, T., Malik, J., Aditiawati, P., & Sulistyono. (2022). Study of Characterization of Activated Carbon from Coconut Shells on Various Particle Scales as Filler Agent in Composite Materials. *Journal of the Korean Wood Science and Technology*, *50*(4), 256–271. https://doi.org/10.5658/WOOD.2022.50.4.256.

[25] Moraes, C. A. M., Fernandes, I. J., Calheiro, D., Kieling, A. G., Brehm, F. A., Rigon, M. R., Berwanger Filho, J. A., Schneider, I. A. H., & Osorio, E. (2014). Review of the rice production cycle: By-products and the main applications focusing on rice husk combustion and ash recycling. *32*(11), 1034–1048. https://doi.org/10.1177/0734242X14557379.

[26] Pode, R. (2016). Potential applications of rice husk ash waste from rice husk biomass power plant. *Renewable and Sustainable Energy Reviews*, *53*, 1468–1485. https://doi.org/10.1016/J.RSER.2015.09.051.

[27] Bazan-Wozniak, A., Cielecka-Piontek, J., Nosal-Wiercińska, A., & Pietrzak, R. (2022). Adsorption of Organic Compounds on Adsorbents Obtained with the Use of Microwave Heating. *Materials*, *15*(16). https://doi.org/10.3390/MA15165664/S1.

[28] Sujiono, E. H., Zabrian, D., Zurnansyah, Mulyati, Zharvan, V., Samnur, & Humairah, N. A. (2022). Fabrication and characterization of coconut shell activated carbon using variation chemical activation for wastewater treatment application. *Results in Chemistry*, *4*, 100291. https://doi.org/10.1016/J.RECHEM.2022.100291.

[29] Wang, J., Ma, J., & Sun, Y. (2022). Adsorption of Methylene Blue by Coal-Based Activated Carbon in High-Salt Wastewater. *Water 2022, Vol. 14, Page 3576*, *14*(21), 3576. https://doi.org/10.3390/W14213576.

[30] Mbarki, F., Selmi, T., Kesraoui, A., & Seffen, M. (2022). Low-cost activated carbon preparation from Corn stigmata fibers chemically activated using H3PO4, ZnCl2 and KOH: Study of methylene blue adsorption, stochastic isotherm and fractal kinetic. *Industrial Crops and Products*, *178*, 114546. https://doi.org/10.1016/J.INDCROP.2022.114546.

[31] Hu, Q., Xu, Z., Qiao, S., Haghseresht, F., Wilson, M., & Lu, G. Q. (2007). A novel color removal adsorbent from heterocoagulation of cationic and anionic clays. *Journal of Colloid and Interface Science*, *308*(1), 191–199. https://doi.org/10.1016/J.JCIS.2006.12.052.

[32] Kalam, S., Abu-Khamsin, S. A., Kamal, M. S., & Patil, S. (2021). Surfactant Adsorption Isotherms: A Review. *ACS Omega*, *6*(48), 32342. https://doi.org/10.1021/ACSOMEGA.1C04661.

[33] Hambisa, A. A., Regasa, M. B., Ejigu, H. G., & Senbeto, C. B. (2023). Adsorption studies of methyl orange dye removal from aqueous solution using Anchote peel-based agricultural waste adsorbent. *Applied Water Science*, *13*(1), 1–11. https://doi.org/10.1007/S13201-022-01832-Y/TABLES/4.

[34] Hasani, N., Selimi, T., Mele, A., Thaçi, V., Halili, J., Berisha, A., & Sadiku, M. (2022). Theoretical, Equilibrium, Kinetics and Thermodynamic Investigations of Methylene Blue Adsorption onto Lignite Coal. *Molecules 2022, Vol. 27, Page 1856*, *27*(6), 1856. https://doi.org/10.3390/MOLECULES27061856.

[35] Lestari, D. I., Yuliansyah, A. T., & Budiman, A. (2022). Adsorption studies of KOH-modified hydrochar derived from sugarcane bagasse for dye removal: Kinetic, isotherm, and thermodynamic study. *Communications in Science and Technology*, *7*(1), 15–22. https://doi.org/10.21924/CST.7.1.2022.669.

[36] Fathi Hasanbarogh, A., Ghasemi, N., & Ezzatzadeh, E. (2022). Kinetic and thermodynamic studies of Methylene Blue adsorption process from aqueous solutions by MIL-101(Cr)@ZnO nanostructure. *Https://Doi.Org/10.1080/03067319.2022.2115898*.

[37] Keleşoğlu, S., Kes, M., Sütçü, L., & Polat, H. (2012). Adsorption of Methylene Blue from Aqueous Solution on High Lime Fly Ash: Kinetic, Equilibrium, and Thermodynamic Studies. *Journal of Dispersion Science and Technology*, *33*(1), 15–23. https://doi.org/10.1080/01932691.2010.528677.

[38] Ugraskan, V., Isik, B., & Yazici, O. (2022). Adsorptive removal of methylene blue from aqueous solutions by porous boron carbide: isotherm, kinetic and thermodynamic studies. *Chemical Engineering Communications*, *209*(8), 1111–1129. https://doi.org/10.1080/00986445.2021.1948406.

[39] Abbas, M., & Trari, M. (2020). Removal of Methylene Blue in Aqueous Solution by Economic Adsorbent Derived from Apricot Stone Activated Carbon. *Fibers and Polymers*, *21*(4), 810–820. https://doi.org/10.1007/S12221-020-8630-8.

[40] Touzani, I., Fikri-Benbrahim, K., Ahlafi, H., Ihssane, B., & Boudouch, O. (2022). Characterization of Ziziphus lotus' Activated Carbon and Evaluation of Its Adsorption Potential. *Journal of Environmental and Public Health*, *2022*. https://doi.org/10.1155/2022/8502211.

[41] Li, X., Qiu, J., Hu, Y., Ren, X., He, L., Zhao, N., Ye, T., & Zhao, X. (2020). Characterization and comparison of walnut shells-based activated carbons and their adsorptive properties. *Adsorption Science and Technology*, *38*(9–10), 450–463. https://doi.org/10.1177/0263617420946524.

[42] Wang, Y. X., Ngo, H. H., & Guo, W. S. (2015). Preparation of a specific bamboo based activated carbon and its application for ciprofloxacin removal. *Science of the Total Environment*, *533*, 32–39. https://doi.org/10.1016/J.SCITOTENV.2015.06.087.

[43] Kyzas, G. Z., Deliyanni, E. A., & Matis, K. A. (2016). Activated carbons produced by pyrolysis of waste potato peels: Cobaltions removal by adsorption. *Colloids and Surfaces A: Physicochemical and Engineering Aspects*, *490*, 74–83. https://doi.org/10.1016/J.COLSURFA.2015.11.038.

[44] Han, Q., Wang, J., Goodman, B. A., Xie, J., & Liu, Z. (2020). High adsorption of methylene blue by activated carbon prepared from phosphoric acid treated eucalyptus residue. *Powder Technology*, *366*, 239–248. https://doi.org/10.1016/J.POWTEC.2020.02.013.

[45] Đurović-Pejčev, R., Radmanović, S., Tomić, Z. P., Kaluđerović, L., & Đorđević, T. (2023). Characterization of the clomazone sorption process in four agricultural soils using different kinetic models. *Environmental Science: Processes & Impacts*, *25*(3), 542–553. https://doi.org/10.1039/D2EM00272H.

[46] Zhang, N., Reguyal, F., Praneeth, S., & Sarmah, A. K. (2023). A novel green synthesized magnetic biochar from white tea residue for the removal of Pb(II) and Cd(II) from aqueous solution: Regeneration and sorption mechanism. *Environmental Pollution*, *330*, 121806. https://doi.org/10.1016/J.ENVPOL.2023.121806.

[47] Gürkan, E. H., İlyas, B., & Tibet, Y. (2022). Adsorption of Cu(II) ve Zn(II) ions by alginate-based composites: Full factorial design approach. *Fullerenes Nanotubes and Carbon Nanostructures*, *30*(8), 787–800. https://doi.org/10.1080/1536383X.2021.2021891.

[48] Gürkan, E. H., İlyas, B., & Tibet, Y. (2021). Adsorption performance of heavy metal ions from aqueous solutions by a waste biomass based hydrogel: comparison of isotherm and kinetic models. *Https://Doi.Org/10.1080/03067319.2021.1873314*.

[49] El-Shafey, E. I. (2007). Sorption of Cd(II) and Se(IV) from aqueous solution using modified rice husk. *Journal of Hazardous Materials*, *147*(1–2), 546–555. https://doi.org/10.1016/J.JHAZMAT.2007.01.051.

[50] Mousavi, S. A., Shahbazi, D., Mahmoudi, A., & Darvishi, P. (2022). Methylene blue removal using prepared activated carbon from grape wood wastes: adsorption process analysis and modeling. *Water Quality Research Journal*, *57*(1), 1–19. https://doi.org/10.2166/WQRJ.2021.015.

[51] Chung, J., Sharma, N., Kim, M., & yun, kyusik. (2022). Activated Carbon Derived from Sucrose and Melamine as Low-Cost Adsorbent with High Adsorption Capacity for Removal of Methylene Blue in Wastewaters. *SSRN Electronic Journal*. https://doi.org/10.2139/SSRN.3976703.

[52] Mu, W., Bao, D., Chang, C., & Lian, F. (2020). Adsorption of Methyl Blue by Maize Waste Based Biochar: Adsorption Kinetics and Isotherms. *J. Phys*. https://doi.org/10.1088/1742-6596/1622/1/012081.

[53] Pelekani, C., & Snoeyink, V. L. (2000). Competitive adsorption between atrazine and methylene blue on activated carbon: The importance of pore size distribution. *Carbon*, *38*(10), 1423–1436. https://doi.org/10.1016/S0008-6223(99)00261-4.

[54] Kim, C. H., Yang, C. M., Kim, Y. A., & Yang, K. S. (2019). Pore engineering of nanoporous carbon nanofibers toward enhanced supercapacitor performance. *Applied Surface Science*, *497*, 143693. https://doi.org/10.1016/J.APSUSC.2019.143693.

[55] Ahmad, M. A., Mohamad Yusop, M. F., Zakaria, R., Karim, J., Yahaya, N. K. E. M., Mohamed Yusoff, M. A., Hashim, N. H. F., & Abdullah, N. S. (2021). Adsorption of methylene blue from aqueous solution by peanut shell based activated carbon. *Materials Today: Proceedings*, *47*, 1246–1251. https://doi.org/10.1016/J.MATPR.2021.02.789.

[56] Shaaban, A., Se, S. M., Mitan, N. M. M., & Dimin, M. F. (2013). Characterization of Biochar Derived from Rubber Wood Sawdust through Slow Pyrolysis on Surface Porosities and Functional Groups. *Procedia Engineering*, *68*, 365–371. https://doi.org/10.1016/J.PROENG.2013.12.193.

[57] Takagi, H., Maruyama, K., Yoshizawa, N., Yamada, Y., & Sato, Y. (2004). XRD analysis of carbon stacking structure in coal during heat treatment. *Fuel*, *83*(17–18), 2427–2433. https://doi.org/10.1016/J.FUEL.2004.06.019.

[58] Liu, Y., Zhao, X., Li, J., Ma, D., & Han, R. (2012). Characterization of bio-char from pyrolysis of wheat straw and its evaluation on methylene blue adsorption. *New Pub: Balaban*, *46*(1–3), 115–123. https://doi.org/10.1080/19443994.2012.677408.